A Metabolite Responsive Nanoparticle-Protein Complex.

Krista R. Fruehauf[a], Tae Il Kim[b], Edward L. Nelson[c], Joseph P. Patterson[a], Szu-Wen Wang[b], and Kenneth J. Shea[a]**

[a] Department of Chemistry, University of California, Irvine (UCI), Irvine, California, 92697-2025, USA

[b] Department of Chemical and Biomolecular Engineering, University of California, Irvine (UCI), Irvine, California, 92697-2580, USA

[c] Department of Medicine, Chao Family Comprehensive Cancer Center, and Institute for Immunology, University of California, Irvine (UCI), Orange, California, 92868, USA

* co-corresponding authors

Abstract

Stimuli responsive polymers are an efficient means of targeted therapy. Compared to conventional agents, they increase bioavailability and efficacy. In particular, polymer hydrogel nanoparticles (NPs) can be designed to respond when exposed to a specific environmental stimulus such as pH or temperature. However, targeting a specific metabolite as the trigger for stimuli response could further elevate selectivity and create a new class of bioresponsive materials. In this work we describe an *N*-isopropylacrylamide (NIPAm) NP that responds to a specific metabolite characteristic of a hypoxic environment found in cancerous tumors. NIPAm NPs were synthesized by copolymerization with an oxamate derivative, a known inhibitor of lactate dehydrogenase (LDH). The oxamate functionalized NPs (OxNP) efficiently sequestered LDH to produce an OxNP-protein complex. When exposed to elevated concentrations of lactic acid, a substrate of LDH and a metabolite characteristic of hypoxic tumor microenvironments, OxNP-LDH complexes swelled (65%). The OxNP-LDH complexes were not responsive to structurally related small molecules. This work demonstrates a proof of concept for tuning NP responsiveness by conjugation with a key protein to target a specific metabolite of disease.

Introduction

Drug delivery has been a high priority for researchers in academia and industry alike. Challenges arise from solubilizing drugs, maximizing bioavailability, and ensuring selectivity toward the tissues and organs that are to be treated. However, combining these traits into a single vehicle remains elusive and has been a driving force for research. Methods devised to address these problems include developing stimuli-responsive materials. This strategy addresses the challenges of selectivity and if designed appropriately, can help increase bioavailability.

Various strategies have been investigated including systems responsive to changes in pH[1-10], reducing or oxidizing environments[11], disease associated enzymes[12-16] or small molecules[17], hypoxic environments[18], mechanical cues[19,20], and temperature[21,22]. However, the relatively low incidence of clinical success would suggest there are still opportunities to improve performance.[23,24] Other methods draw inspiration from biology. Protein-polymer conjugates have made an impact in the scientific community as an attractive approach to address drug delivery. These strategies consist of non-covalent, covalent, and supramolecular interactions between polymers and proteins. Some examples involve protein cages, formation of polymer micelles around proteins, and synthesis of nanoparticles incorporating proteins into the backbone.[25-32] All of these strategies have been used to enhance the success and selectivity of delivering biological agents as well as drugs.

The versatility of nanoparticles allows for a range of approaches to be employed. Protein-nanoparticle complexes are of particular interest as treatments for various diseases, especially cancer. The stimuli response of protein-nanoparticle complexes has depended on many of the previously mentioned strategies. These studies have included adenosine-5'-triphosphate (ATP) and glucose responsive systems.[33] Both the ATP and glucose systems rely on a concentration

gradient or an intra- and intercellular difference in concentration of these molecules. The specificity of these systems is lacking in the sense that ATP and glucose are found throughout the body. High local concentration of a specific molecule or metabolite that is a signature of a disease can provide a chemospecific target for therapeutic intervention. However, there remains a compelling need to develop a responsive polymer-protein conjugated system designed around a specific disease associated metabolite. Designing a protein-nanoparticle complex that responds to a metabolite of disease could provide an effective solution to the issue of selectivity. By focusing on a molecule or metabolite that has distinctively high concentrations in the local area of disease, side effects can be minimized while maximizing therapeutic effects.

There have been many studies describing the Warburg effect in cancer progression. This phenomenon describes an accumulation of lactate, leading to a decrease in pH within the cancer microenvironment.[34-36] The phenomenon is attributed to cancer cells that predominantly utilize anaerobic glycolysis instead of oxidative phosphorylation.[34-36] Cancer usually exists under low oxygen, or hypoxic, conditions so cells must compensate for this impediment to energy production. This leads to a lactate concentration higher than what is found under normoxic conditions. Anaerobic glycolysis is performed in healthy tissues as well, most notably during exercise when a build-up of lactic acid occurs. Healthy tissues have lactate concentrations between 0.5-2 mM[37-39], while concentrations in tumor tissues range from 10-20 mM[40-43] and up to 40 mM[35,40]. The almost ten-fold increase in lactic acid lowers the pH from 7.4 to 6.0-7.0[44] an effect that has been taken advantage of by designing polymers that release anti-cancer drugs under acidic conditions.[34-36] However, there are organs with regions of low pH that are not associated with cancer, most notably the stomach and kidney. A more chemospecific trigger, such as one that responds to high lactate concentrations, would be more effective.

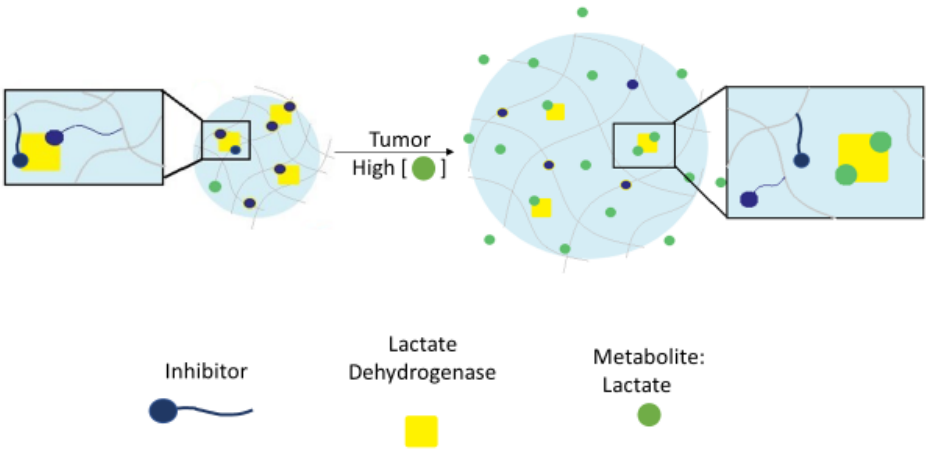

Figure 1: Lactate responsive nanoparticle. An inhibitor for LDH is incorporated into the NP. When LDH is introduced, the inhibitor acts as a cross-linker between the particle and protein leading to a decrease in NP size. Once the complex is introduced to lactate, the inhibitor is displaced and the cross-linking is eliminated. This leads to a swelling of the particle.

In this report, we describe hydrogel nanoparticles (NP) that are responsive to lactate at physiologically relevant concentrations. To achieve this, we incorporated a known inhibitor of lactate dehydrogenase (LDH), oxamate, into the backbone of a hydrogel polymer. The polymer bound oxamate was used to bind LDH, present as a homomeric tetramer, non-covalently to the polymer and function as a cross-linker between the polymer NP and LDH. We utilized *N*-isopropylacrylamide (NIPAm) as the base monomer. NIPAm was chosen due to its low affinity for plasma proteins, this minimizes any non-specific binding of proteins other than the one of interest.[45] NIPAm polymers exhibit a lower critical solution temperature (LCST) at approximately 32 ^{o}C. Below this temperature, the polymer is solvent swollen. Increasing the temperature beyond 32 ^{o}C desolvates the particle, leading to a volume reduction. Our design strategy was to incorporate LDH into the polymer in its solvent swollen state (< 32 ^{o}C) before raising the temperature to physiological conditions.

Our LDH was based on the protein sequence of *Bacillus stearothermophilus* LDH, a thermally stable and well characterized protein that would be compatible with experimental

conditions. LDH is a homomeric tetramer with four binding sites and provides a nexus for cross-linking by the polymer-bound oxamate (Figure 1). This enzyme converts pyruvate into lactate, this is done at higher than normal rates within the tumor microenvironment so the cancer cells can utilize lactate fermentation. However, this enzymatic reaction is reversible, and lactate can be converted back into pyruvate with the same enzyme. The polymer-bound oxamate will non-covalently bind LDH; when more than one oxamate binds to the homomeric tetramer, the result is cross-linking. These cross-links will be competitively displaced by lactate upon entering an environment with elevated lactate levels. The decreased cross-linking of the polymer to LDH endows the particle with a lactate responsiveness that results in NP swelling. At appropriate loadings of inhibitor and LDH, one can tune the lactate responsiveness of the NP to the relevant physiological range of lactate in the local cancer environment.

Experimental

^{1}H NMR spectra were recorded at 500 MHz, using a Bruker DRX 500 spectrometer. ^{13}C NMR spectra were recorded at 125 MHz, using a Bruker DRX CRYO500 spectrometer. ^{1}H NMR and ^{13}C NMR spectra were run in $CDCl_3$ with shifts reported as δ values in ppm and referenced to residual solvent proton or carbon. Splitting patterns are abbreviated as follows: s = singlet, d = doublet, dd = doublet of doublets, t = triplet, q = quartet, quint = quintet, sext = sextet, sep = septet, m = multiplet, br = broad.

General Procedures.

Methylene chloride was obtained from a dry Solvent Dispensing System. Chloroform was distilled and kept under nitrogen. Amine bases were freshly distilled over CaH_2 from a ketal

still. NIPAm was recrystallized from hexanes. All other commercial reagents were used as received. Reactions were monitored by thin layer chromatography using glass-backed EM Science Silica Gel 60 PF254 Plates. Flash chromatography was performed using EM Science Silica Gel 60 (230-400 mesh). All volatile solvents were removed, *in vacuo*, under reduced pressure using a Büchi rotary evaporator.

Inhibitor Synthesis

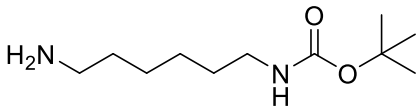

1-Boc-1,6 hexanediamine **2**: A solution of 1,6-hexanediamine (11g, 100 mmol) in chloroform (26 mL) was cooled to 0 ^{o}C with an external ice bath then treated via dropwise addition over two hours with a solution of Boc anhydride (4.4 g, 20 mmol) in chloroform (20 mL). Reaction was removed from ice and allowed to warm to room temperature. After reacting overnight, the solution was filtered, filtrate concentrated *in vacuo*, re-dissolved in ethyl acetate, washed with brine (3 x), dried over $MgSO_4$, filtered, then concentrated *in vacuo*. Flash column chromatography was performed and eluted with methylene chloride treated with an equal volume of methanol:ammonium hydroxide solution then concentrated *in vacuo* to yield 4.5 g (81%) of a thick white oil. ^{1}H, ^{13}C NMR, and HRMS matched the literature values.[46]

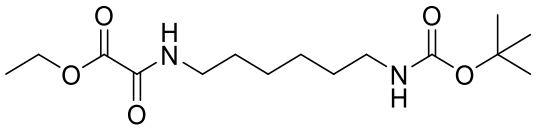

Oxamide ester **3**: To a cooled solution of ethyl chlorooxoacetate (0.08 mL, 0.75 mmol) in chloroform (2 mL) at 0^{o}C, a solution of **2** (165 mg, 0.75 mmol) and Hünig's base (0.2 mL, 1.125 mmol) in chloroform (3 mL) was added. Reaction turned from clear to light yellow. After

completion by TLC, solution was washed with 0.1 N HCl (1 x), washed with DI water (1 x), dried over $MgSO_4$, filtered, and concentrated *in vacuo*. Flash column chromatography was performed eluting with 4:6 hexanes to ethyl acetate to yield 156.6 mg (66%) of a light yellow oil. ^{1}H NMR ($CDCl_3$-D + 0.05% TMS, 500 MHz): δ/ppm = 7.21 (s, 1H, NH), 4.57 (s, 1H, NH), 4.39 (q, 2H, CH_2-O), 3.39 (q, 2H, CH_2-NH), 3.16 (d, 2H, CH_2-NH), 1.5 (m, 12H, CH_3), 1.35-1.47 (m, 8H, CH_2-CH_2); ^{13}C NMR ($CDCl_3$-D + 0.05% TMS, Cryo 500 MHz): δ 160.9, 156.6, 156.0, 63.3, 40.3, 39.7, 30.0, 29.1, 28.4, 26.3, 26.2, 14.0, 13.9; HRMS (ESI-TOF): *m/z* calcd for $C_{15}H_{28}N_2O_5$ $[M + Na]^+$ 339.1896; found 339.1892.

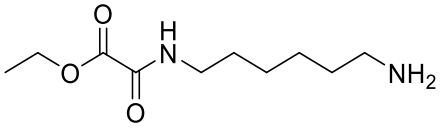

Boc Deprotection **4**: A solution of compound **3** (24 mg, 0.079 mmol) in methylene chloride (0.3 mL) was treated with TFA (0.2 mL, 2.7 mmol) at room temperature. The reaction was monitored by TLC and finished in 30 min. Solvent was removed to produce a TFA salt, 20 mg (80% yield). ^{1}H NMR ($CDCl_3$-D + 0.05% TMS, 500 MHz): δ/ppm = 4.42 (q, 2H), 3.43 (m, 2H), 3.17 (m, 2H) 1.79-1.54 (m, 13H); ^{13}C NMR ($CDCl_3$-D, Cryo 500 MHz): δ 158.8, 158.5, 117.0, 114.7, 62.1, 62.0, 61.9, 54.4, 54.1, 13.35; HRMS (ESI-TOF): *m/z* calcd for $C_{10}H_{20}N_2O_3$ $[M + H]^+$ 217.1552; found 217.1550.

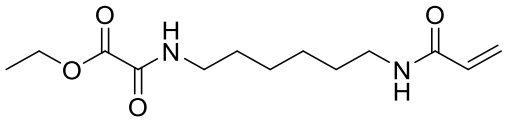

Acryloylation **5**: Et_3N (0.65 mL, 4.5 mmol) was added to compound **4** (125 mg, 0.38 mmol) at 0^{o}C. Then, a solution of acryloyl chloride (36 µL, 0.45 mmol) in CH_2Cl_2 (5 mL) was added and stirred for 1h at 0^{o}C. The reaction then came to rt and left to stir o/n. Reaction was complete by TLC (ethyl acetate, R_f = 0.25) and washed with NH_4Cl (1x), $NaHCO_3$ (1x), NaCl (1x), then dried

over $MgSO_4$, filtered, and concentrated *in vacuo.* Flash column chromatography in EtOAc was performed to produce 54.8 mg (53 % yield). ^{1}H NMR ($CDCl_3$-D + 0.05% TMS, 500 MHz): δ/ppm = 7.22 (1H, b), 6.33 (dd, 1H, CH_{sp2}), 6.16 (dd, 1H, CH_{sp2}), 5.69 (dd, 1H, CH_{sp2}), 4.41 (d, 1H, NH), 3.39 (q, 2H, CH_2-O), 1.65-1.45 (m, 11H, CH_2-CH_2); ^{13}C NMR ($CDCl_3$-D + 0.05% TMS, Cryo 500 MHz): δ 130.9, 126.3, 63.2, 39.5, 39.2, 29.4, 29.0, 26.2, 14.0; HRMS (ESI-TOF): *m/z* calcd for $C_{13}H_{22}N_2O_4$ $[M+Na]^+$ 293.1477; found 293.1475.

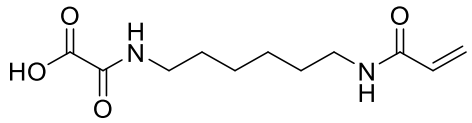

Ester hydrolysis **6**: KOH (18 mg, 0.32 mmol) was added to a solution of **5** (43 mg, 0.16 mmol) in MeOH (2 mL) at rt. Reaction complete by TLC (ethyl acetate) after 10 min (R_f = 0). Reaction mixture was acidified with 5 N HCl. Solvent removed to produce a white solid (quantitative yield). ^{1}H NMR ($CDCl_3$-D + 0.05% TMS, 500 MHz): δ/ppm = 8.83 (s, 1H), 8.11 (s, 1H), 6.2 (dd, 1H, CH_{sp2}), 6.09 (dd, 1H), 5.58 (dd, 1H, CH_{sp2}), 3.11 (m, 4H, CH_2) 1.44-1.28 (m, 8H, CH_2); ^{13}C NMR ($CDCl_3$-D +0.05% TMS, Cryo 500 MHz): δ 128.8, 31.9. 29.4, 28.47, 26.1, 22.7, 14.1; HRMS (ESI-TOF): *m/z* calcd for $C_{11}H_{18}N_2O_4$ $[M-H]^-$ 241.1188; found 241.1188.

OxNP Characterization

DLS was run using OxNPs diluted 10-fold into nanopure water. Samples at 37 ^{o}C were equilibrated for 2 min before measuring. Molecular weight of nanoparticles was determined using SEC-MALS (Malvern Viskotek GPC/SEC triple detection system). The system was run in PBS (10 mM phosphate, 50 mM NaCl). The column (Viscotek A7000) was heated to 30 ^{o}C and the system was calibrated to a 500 kDa pullulan standard. Nanoparticle samples were prepared by dialyzing in PBS overnight. The OxNP sample was diluted into PBS (2.5 mg/mL) and

injected onto the column. Injections of 40 μL were used with a flow rate of 1 mL/min. The M_n was determined to be 2.276 x 10^8 and M_w was 2.863 x 10^8 with a PDI of 1.26.

Cloning of LDH gene

DNA encoding wtLDH from *B. stearothermophilus* with a N-terminal His6X tag was synthesized by Integrated DNA Technologies using sequences optimized for *E. coli* expression. *B. stearothermophilus* LDH was selected due to its structural stability at elevated temperature. The gene was ligated into Blunt Topo vector, transformed into *E. coli* (DH5α) cells, and sequence confirmed with standard Sanger's sequencing (GeneWiz). wtLDH fragment of the wtLDH-TOPO vector was digested with *BamHI* and *NdeI*, extracted from a 0.7% agarose gel (GeneJET kit), and ligated into a *BamHI*- and *NdeI*-digested pET11a vector. The ligated plasmid was co-transformed into BL21(DE3) *E. coli* cells together with a pGRO7 chaperone protein plasmid.

Purification of LDH

Single colonies of co-transformed BL21(DE3) cells were picked and incubated overnight at 37°C for 16-18 hrs, and overnights were reinoculated into 1 L of LB culture containing 100 μg/ml ampicillin, 50 μg/ml chloramphenicol and 1 mM arabinose (to induce the expression of GroEL/ES chaperone proteins). Once the OD600 of the culture reached 0.6-0.7, the LDH expression was induced with 1 mM IPTG for 3 hrs, and cells were harvested. Cells were resuspended in breaking buffer and lysed in French pressure cell. Cell debris and insoluble fractions were removed using ultracentrifuge, and soluble fractions were purified using HisPur Ni-NTA affinity column following the product protocols. Samples of each fraction from the

affinity column were run on SDS-PAGE. The elution fractions with soluble LDH proteins were combined and exchanged into phosphate buffer using Zeba Desalting columns. The concentration of the purified LDH was obtained with a micro BCA Kit and stored at -80 °C.

Protein Characterization

Characterization of LDH was based on prior protocols for thermophilic proteins derived from *B. stearothermophilus.*[47] In summary, purified LDH was run on 12% SDS-PAGE gel to examine the presence of impurities during and after purification. Mass spectroscopy was also performed (Waters Quattro Premier XE) to verify molecular weight of purified LDH. The secondary structure and thermostability of LDH were obtained following the protocol of Dalmau et al.[47] Jasco 810 spectropolarimeter equipped with Jasco Peltier temperature controller (Jasco, Easton, MD) were used to measure the far-UV circular dichroism (CD). LDH proteins were examined at a concentration of 0.06 mg/ml in 50 mM potassium phosphate and 100 mM NaCl. Samples were scanned between 200 and 260 nm at 25 °C at scanning speed of 10 nm/min in 0.1 cm pathlength quartz cells.

Thawed cells were resuspended in buffer (20 mM Tris pH 8.7, 0.02% sodium azide, 2 U/mL DNase, 2 U/mL RNase, 1 mM $MgCl_2$ and 1 mM PMSF) and lysed in a French pressure cell (Thermo Scientific, Milford, MA). The insoluble fraction was removed by ultracentrifugation. The resulting supernatant was heated at 70 ^{o}C for 20 min and the native, denatured E. coli protein aggregates were removed by centrifugation. The recovered supernatant was loaded onto a HiPrep Q-sepha rose anion exchange column (GE Healthcare, Piscataway, NJ) previously equilibrated with Tris buffer (20 mM Tris pH 8.7, 0.02% sodium azide, and 5 mM EDTA).

LDH Kinetics

Protocols for determining K_{cat} and K_m of LDH were based on previous studies by Clarke et al.[48] Enzyme kinetics were measured by absorbance increases at 340 nm in the generation of NADH. All assays were done at 25 °C and in 100 mM triethanolamine hydrochloride buffer. Enzyme at 100 nM was mixed with 10 mM NAD^+ and 20 mM FBP with varying lactate concentrations. The initial slope of the absorbance vs. time was obtained for a range of lactate concentrations. This initial slope vs. concentration of lactate was plotted in GraphPad Prism and kinetic parameters (K_m and k_{cat}) were determined using a non-linear curve fit to the Michaelis-Menten equation.

Quantification of LDH Uptake

A 1 mL sample of NP (0.4 mg/mL), FBP (1 mM), NAD^+ (1 mM), and LDH (0.35 mg/mL) was prepared in nanopure water. Control samples consisted of NIPAm NPs (0.4 mg/mL) with LDH (0.35 mg/mL) and FBP (1 mM). After LDH was incubated with its coenzymes in water (1 min), NP was added. After incubating at rt for 30 min, the samples were heated in a water bath at 37 ^oC for 10 min followed by centrifugation for 10 min at 14,000 rpm. For samples that were not incubated at 37 ^oC, they incubated at room temperature for an additional 10 min before centrifugation. A white pellet formed at the bottom of the centrifuge tube and the supernatant was collected for fluorescence measurements. Measurements were taken in quartz cuvettes (Starna Cells, 3mm) on a Cary Eclipse Spectrometer. Excitation was set to 280 nm and emission was measured from 290 nm to 400 nm, RFU measurements were

recorded at 342 nm. A calibration curve of LDH was created starting at 0.01 mg/mL ending at 0.35 mg/mL.

The number of proteins bound to OxNPs was calculated using the wt/wt ratio of proteins bound to NPs. Using the respective molecular weights (M_n for the OxNPs), the mole to mole ratio was calculated. Using Avogadro's number, we were then able to calculate the exact number of LDH proteins per OxNP. Determining density of OxNPs required the molar mass of OxNPs and the Z-Average value to determine the volume. The molar mass of one OxNP was calculated as stated above using M_n and Avogadro's number, this value was then divided by the volume of an OxNP. To determine the percent volume of OxNP taken up by LDH, we divided the volume of 1000 LDH proteins by the volume of OxNP. The volume of LDH was calculated using the mass of one LDH protein divided by its density. The mass of one LDH protein was calculated using the molecular weight of LDH divided by Avogadro's number.

Circular Dichroism of NPs with LDH

Measurements were carried out on a Jasco J-380 spectrometer. Continuous scanning was used with a speed of 20 nm/min at increments of 1 nm from 200 nm to 260 nm. Baseline correction was used with a 2 nm bandwidth. All data are an average of three scans. Phosphate buffer (150 mM) was used for baseline correction. Samples (200 μL) consisted of FBP (1 mM), NAD^+ (0.5 mM), LDH (0.6 mg/mL), and OxNPs (0.1 mg/mL) in phosphate buffer (150 mM). Measurements were carried out at room temperature and 37 ^oC. For measurements performed at elevated temperatures, samples incubated for 10 min before measuring. Controls were taken of LDH and OxNPs individually. OxNP controls did not include any coenzymes and were taken in

phosphate buffer (150 mM). LDH controls were performed with necessary coenzymes in phosphate buffer (150 mM).

Response of OxNPs to Small Molecules

Solutions (1 mL) were made consisting of OxNP (0.4 mg/mL) and small molecules (10 mM) in nanopure water. Samples incubated for 5-10 min at rt before being measured. DLS measurements at 25 ^{o}C were performed in triplicate and the average was taken to determine the hydrodynamic diameter. Samples were then incubated for 2 min at 37 ^{o}C before repeating measurements in triplicate. It was visually apparent that particles were above LCST as the solution became turbid with turbidity increasing with the size of the particles.

The size change was converted to percent change in volume using the size of OxNP as the standard. This was determined by calculating the volume of OxNPs with small molecules based on their Z-Average. This was subtracted from the volume of OxNP and divided by the volume of OxNP using Equation 1. OxNP percent change in volume was set as 0.

Equation 1. $\%\ Change\ in\ volume = \frac{(Volume\ of\ OxNP\ with\ Small\ Molecule - Volume\ of\ OxNP)}{Volume\ of\ OxNP}$

Response of OxNP-LDH Complexes to Small Molecules

Solutions (1 mL) were made consisting of OxNP, FBP (1 mM), NAD^{+} (1 mM), and LDH (0.175 mg/mL). The control sample consisted of NIPAm NPs (0.4 mg/mL) in water. NAD^{+}, FBP, and LDH were incubated together in water for 1 min before adding NP. Samples were incubated at rt for 10 min before taking DLS measurements at 25 ^{o}C. Measurements were performed in triplicate and the average was taken to determine the hydrodynamic diameter. Samples were then incubated for 2 min at 37 ^{o}C before repeating measurements in triplicate. It

was visually apparent that particles were above LCST as the solution became turbid. OxNP-LDH complexes containing small molecules (10 mM) were prepared in a similar manner as above except small molecules were added at rt before measuring. The same procedure was also followed for their DLS measurements. To test whether the addition of lactic acid was temperature dependent, a separate set of experiments were performed in which lactic acid was added at 37 ^{o}C to pre-mixed OxNP-LDH samples. The same procedure as above was performed except OxNP-LDH solutions were not allowed to come to rt before lactic acid was added. Measurements were taken immediately at 37 ^{o}C. The hydrodynamic diameter of NP was the same regardless of whether lactic acid was added at 25 ^{o}C or 37 ^{o}C. The percent change in volume is detailed by Equation 2.

Equation 2. $\%\ Change\ in\ volume = \frac{(Volume\ \ OxNP\ LDH\ with\ Small\ Molecule - Volume\ OxNP\ LDH)}{Volume\ OxNP\ LDH}$

SEM of Inhibitor Functionalized NPs

A stock solution of OxNP (0.4 mg/mL) containing LDH (0.175 mg/mL), FBP (10 mM), and NAD^{+} (5 mM) was diluted ten-fold to a final concentration of 0.04 mg/mL OxNP and 0.0175 mg/mL LDH. OxNP samples were prepared by drop casting a solution of OxNP in water (0.04 mg/mL, 10 μL) onto glass slides which were then heated in the oven at 150 ^{o}C until dry (1 min). OxNP-LDH complexes were prepared by combining OxNP with LDH and coenzymes before diluting to concentrations previously mentioned. The solution was heated to 37 ^{o}C followed by drop casting onto glass slides and drying in the oven. Samples of OxNP with LDH and lactic acid were prepared similarly, but a stock solution of OxNP with LDH was treated with lactic acid before dilution and drop casting. The samples were sputter coated with a thin conductive layer (5 nm) of gold/palladium alloy (Polaron SC7620) to render the surface of the

NP electrically conductive for SEM imaging. Morphological characterization from the SEM (FEI Quanta 3D) was conducted using an electron voltage of 5 kV and a current of 53 pA.

CryoTEM of OxNP-LDH Complexes

Cryo-TEM samples were prepared by depositing 3 µl sample on a 200 mesh Cu grids with lacey carbon films (Electron Microscopy Sciences). All TEM grids were surface plasma treated for 20 seconds using a Gatan Solarus Advanced Plasma Cleaning System 950 prior to use. An automated vitrification robot (Leica EM GP) was used for plunge vitrification in liquid propane. Cryo-TEM studies were performed on the JEOL JEM 2100F operated at 200 kV, 2k x 2k Gatan CCD camera. Gatan DigitalMicrograph. ImageJ was used for TEM image analysis.

Results and Discussion

Synthesis of Polymerizable Oxamate Derivative

To impart NPs with affinity for LDH, we chose an oxamate derivative as a non-covalent inhibitor. Oxamate is a competitive inhibitor of pyruvate for LDH with a similar K_m as pyruvate

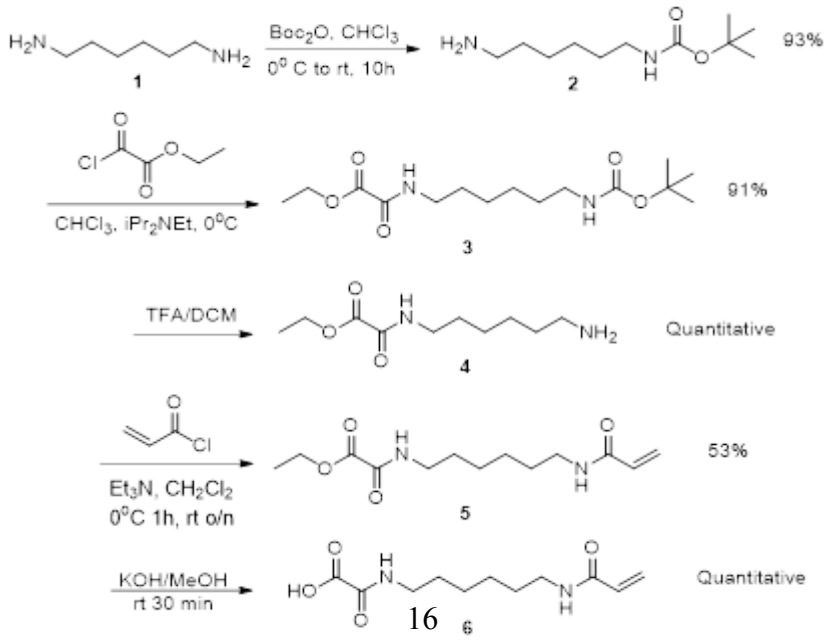

Scheme 1: Synthetic pathway to polymerizable oxamate derivative **6.**

for LDH (0.6 mM).[48] Since attachment of the inhibitor to a polymer backbone can restrict access to the LDH active site, we chose a six carbon atom tether for the oxamate inhibitor. Our choice was based on the successful use of a solid-phase tethered oxamate derivative to purify LDH by affinity chromatography.[49,50] In the chromatographic application, the oxamate moiety was coupled to a 1,6-hexanediamine spacer bound to a Sepharose bead. Drawing from these results, an α,ω-1,6-diamine was functionalized with the oxamate group at the alpha position and an acrylamide at the omega position. In this design, the alpha position can bind to LDH while the omega position can be covalently incorporated into the polymer backbone.

The synthesis of the oxamate derivative **6** (Scheme 1) begins with mono-protection of 1,6 hexanediamine with Boc-anhydride. After purifying the mono-Boc diamine **2** via flash column chromatography, initial efforts to couple oxalic acid to the mono-Boc protected diamine **2** proved challenging, most likely due to the low electrophilicity of oxalic acid. The synthesis was simplified by switching to a more reactive, electrophilic acid chloride ethyl chlorooxoacetate. The free amine was coupled to ethyl chlorooxoacetate in the presence of Hünig's base. The resulting mono-Boc oxamide **3** was then de-protected with TFA in DCM. Following de-protection, acryloylation of the free amine **4** was performed and ester **5** was purified via flash column chromatography. The resulting ethyl ester **5** was then hydrolyzed using KOH in MeOH to produce the oxamate derived monomer **6**.

OxNP Synthesis

The next step was incorporation of **6** into a NIPAm based polymer (Scheme 2). The oxamate functionalized NP (OxNP) formulation consisted of 2 mol % polymerizable oxamate inhibitor **6**, 2 mol % *N,N'*-methylenebis(acrylamide) (Bis) as cross-linker, and 96 mol %

NIPAm. We assumed equal reactivity of NIPAm and the oxamate derivative since both are N-substituted acrylamides.[51] Under these conditions, the feed ratios should reflect the actual incorporation of the monomers in the polymer with random distribution of the oxamate derivative. This is further supported by the high yield of the polymerization (90%). The OxNPs contain an additional permanent cross-linker, 2 mol % Bis. This low-level of covalent cross-linking was included to ensure uniformly sized NPs form but low enough to remain responsive to changes in non-covalent cross-linking between the oxamate and LDH.[52] Using a high concentration of Bis would restrict the polymer chains due to high cross-linking density, making it difficult to observe swelling.

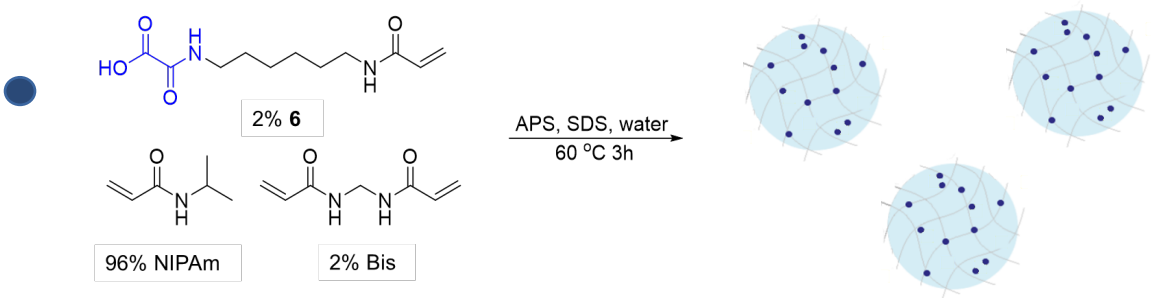

Scheme 2: NP synthesis utilizing 2 mol % polymerizable oxamate inhibitor, 96 mol % NIPAm, and 2 mol % Bis.

OxNPs were synthesized via precipitation polymerization in water and were purified by dialysis for 4 days to remove low molecular weight polymerization byproducts. Following dialysis, the yield of polymers was determined by weighing a lyophilized aliquot of NP solution (90% yield). Dynamic light scattering (DLS) was used to determine the hydrodynamic diameter of the particles and their polydispersity (Experimental Section). Because NIPAm polymers exhibit an LCST ~ 32 °C[30], particle size was measured at both 25 °C and 37 °C. Below the LCST at 25 °C, the hydrodynamic diameter of OxNPs was 403±7 nm. At 37 °C, OxNP diameter decreased to 183±1 nm. Since these particles have intended applications under physiological

conditions, 37 ^{o}C was chosen for all measurements and experimental conditions. Particle size was designed to be at or below 200 nm at body temperature to take advantage of the enhanced permeability and retention effect which promotes accumulation of nanoparticles in tumor tissues and to prevent encumbered circulation.[53]

Quantification of LDH Uptake

Following OxNPs synthesis the next step was to study LDH uptake by OxNPs. The K_m of oxamate for *Bacillus stearothermophillus* LDH is 0.6 mM.[48] For LDH to serve as a cross-link, it must bind to two or more oxamate groups. This is realized under conditions where LDH is present as a homomeric tetramer with four discrete binding sites for oxamate groups. These conditions are realized in the presence of NAD^+ and fructose bisphosphate (FBP)[49,50] which were present in all binding and uptake studies.

OxNPs were incubated with LDH and its coenzymes FBP and NAD^+ at room temperature to allow LDH to diffuse into the solvent swollen OxNPs and bind to the polymer bound oxamate groups. After 30 min at room temperature, samples were heated to 37 ^{o}C for 10 min. Protein uptake was followed by centrifugation of OxNP-LDH complexes, which pelleted at

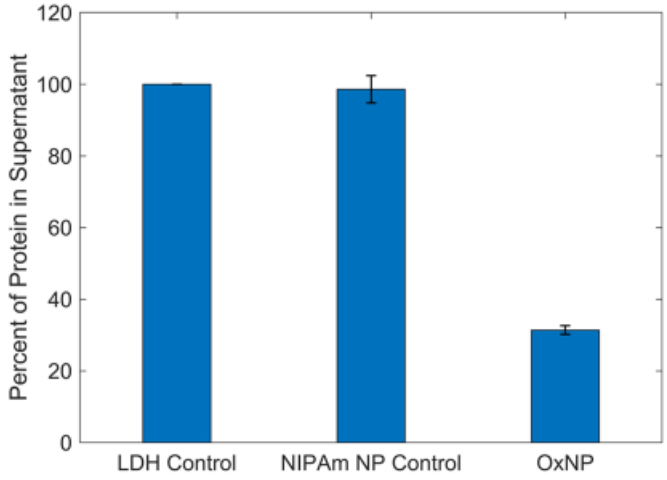

Figure 2: Quantification of LDH uptake by NPs. Centrifugation was performed to pull down NP-LDH complexes leaving the unbound protein free in supernatant. Bars represent amount of LDH leftover in supernatant. LDH Control corresponds to the maximum amount of LDH added to solutions. NIPAm NP Control represents NIPAm NPs without oxamate inhibitor incubated with LDH. OxNP represent NIPAm NPs containing the oxamate inhibitor. The NIPAm NP Control showed no affinity for LDH while the OxNP demonstrated affinity for LDH.

the bottom, leaving unbound LDH in the supernatant. Protein concentration in the supernatant was determined using tryptophan fluorescence (Ex 280 nm, Em 342 nm) standardized against known concentrations of LDH. The results are summarized in Figure 2. Control experiments with unfunctionalized (no oxamate ligands) NIPAm NPs (98 mol % NIPAm and 2 mol % Bis) were included for comparison. OxNPs (0.4 mg/mL) were calculated to bind 0.24 mg/mL of LDH in solution. Control NPs showed negligible LDH uptake. The wt:wt ratio of LDH to OxNPs was calculated to be 0.6 to 1.0. Using size exclusion multi-angle light scattering (SEC-MALS), OxNP molecular weight was determined to be M_n of 2.276 x 10^8, M_w of 2.863 x 10^8, with a PDI of 1.26. Using the known molecular weight of LDH (140 kDa for the tetramer) and OxNP (M_n of 2.276 x 10^8) one calculates approximately 1000 proteins per OxNP. Despite this seemingly large number, less than 1% of the OxNP volume is taken up by LDH. This was derived after determining the density of OxNPs (0.01 g/mL assuming the OxNPs are spherical) and using an assumed density of 1.3 g/mL for LDH.[54] The density calculated for OxNPs does not include the water hydrating the polymer.

Circular Dichroism (CD) Measurements

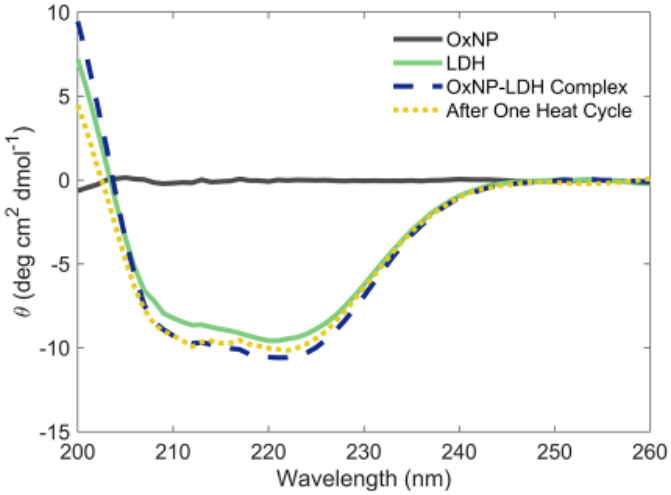

Figure 3: CD Measurements of OxNPs and LDH. CD was performed on OxNP alone and showed no signal. LDH was measured alone as a baseline. OxNP-LDH complexes showed no significant difference from the baseline LDH. After one heat cycle corresponds to measurements of OxNP-LDH complexes after being heated at 37 ^{o}C for 10 minutes followed by cooling and measurement. Each set of conditions demonstrated no denaturation occurring.

Non-covalent complexation of LDH with OxNPs and subsequent thermal cycling of the copolymer-protein complex could subject the protein to structural deformation and/or denaturation. To evaluate this, we used CD spectroscopy to interrogate the OxNP-LDH complex. Samples containing OxNPs alone, LDH alone (both at room temperature and 37 ^{o}C), OxNP-LDH complexes prepared at room temperature, and OxNP-LDH complexes prepared at room temperature followed by heating to 37 ^{o}C and cooling to room temperature were evaluated. In all cases, the alpha helical motifs in LDH were maintained (Figure 3). OxNPs do not disrupt the secondary structure of LDH. These results also indicate that the mechanical distortions from the polymer network's contraction at 37 ^{o}C and expansion at room temperature are insufficient to produce detectable distortions in the non-covalently bound protein.

Response of OxNP to Small Molecules

To establish that the OxNP-LDH complexes are metabolite (lactate) responsive, several controls with OxNPs were performed. DLS was used to monitor the change in size upon exposure of OxNPs to 10 mM solutions of lactic acid and several small molecules containing three or four carbons with either mono- or difunctional carboxylic acid and alcohol moieities at 25 ^{o}C and 37 ^{o}C. We found at 37 ^{o}C, pyruvic acid and oxalic acid caused aggregation (not

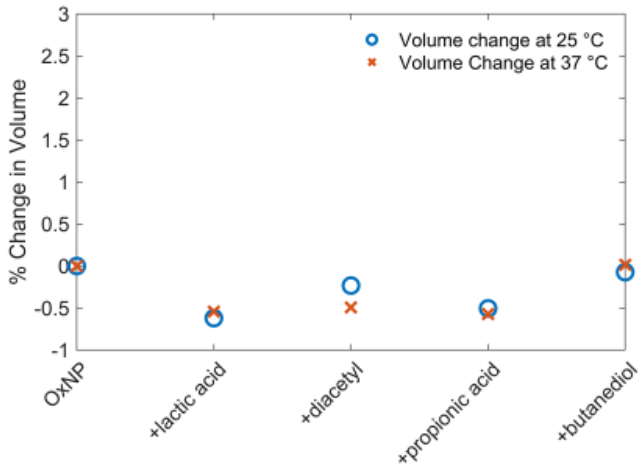

Figure 4: Change in volume of OxNP exposed to small molecules at 25 ^{o}C and 37 ^{o}C. All small molecules had a concentration of 10 mM. Pyruvic acid and oxalic acid not shown.

swelling) of OxNPs, a conclusion supported by the high polydispersity (0.23±0.2 for pyruvic acid and 0.096±0.02 for oxalic acid). Because these two molecules cause aggregation of OxNPs, they were not included in tests on OxNP-LDH complexes. The response of OxNPs to lactic acid, diacetyl, propionic acid, and 2,3-butanediol are shown in Figure 3. None of the small molecules significantly affected the size of OxNPs at 25 ^{o}C or 37 ^{o}C.

Response of OxNP-LDH Complexes to Small Molecules

A similar set of experiments was used to evaluate the response of the NP-protein complexes (OxNP-LDH complexes) to lactic acid and related small molecules. To establish a baseline for the OxNP-LDH complexes, DLS measurements were run in water at 25 ^{o}C and 37

°C. At 25 °C, the complexes had an average size of 308±3 nm and 180±1 nm at 37 °C. One important observation is the change in size of OxNP at 25 °C when LDH is added, the resulting complex is about 100 nm smaller than OxNP by itself (403±7 nm). In contrast, NIPAm NPs do not experience a significant change in size when exposed to LDH at 25 °C (337±8 nm without LDH to 338±5 nm with LDH). The decrease in size of OxNP after exposure to LDH at 25 °C is consistent with the uptake of tetrameric LDH and cross-linking the polymer backbone by binding at least two polymer-bound oxamate moieties. It is reasonable that this shrinkage upon LDH cross-linking would be more apparent when performed in the solvent swollen state (25 °C).

With the preceding benchmarks, the response of OxNP-LDH to small molecules was examined. The conditions were similar to the previous experiment but an additional trial using 1 mM of lactic acid was used to establish if OxNP-LDH complexes exhibit a concentration dependent response to lactic acid. The results, shown in Figure 5, reveal there were no significant changes in volume of OxNP-LDH at 25 °C in the presence of any small molecules at 10 mM concentration.

At 37 °C the volume of OxNP-LDH complexes remained constant with one exception, lactic acid. OxNP-LDH samples treated with 10 mM lactic acid at 37 °C experienced a

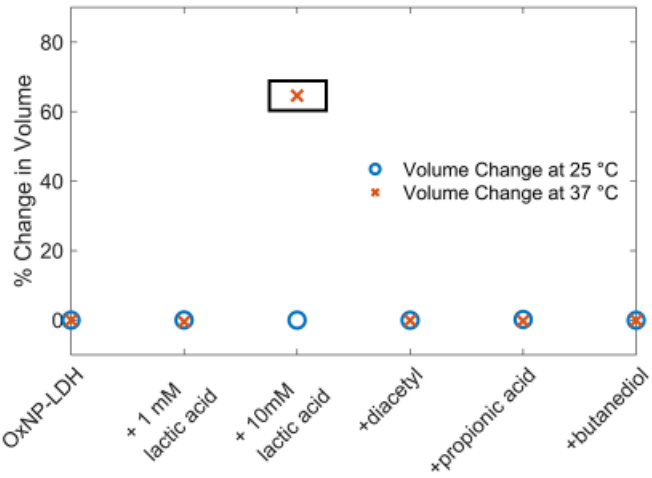

Figure 5: Change in volume of OxNP-LDH complexes exposed to small molecules at 25 °C and 37 °C. Low lactic acid concentrations mirroring those found in healthy tissues (1 mM) do not cause a change in volume. High lactic acid concentrations (10 mM) cause a significant change in volume of OxNP-LDH complexes. The box highlights the data point correlated to a large change in volume at 37 °C. Other small molecules (10 mM) elicited no effect on OxNP-LDH complex volume.

significant increase in volume. In contrast, 1 mM of lactic acid did not influence the volume of OxNP-LDH complexes. We suggest the increase in OxNP-LDH complex volume upon exposure to 10 mM lactic acid arises from a combination of effects which include lactate displacement of the polymer bound oxamate moieties resulting in reduced cross-linking, electrostatic interactions, solvation, and possibly the catalytic activity of LDH. Importantly, we note that 10 mM lactate was the only condition that induced a response.

Due to the sensitivity of NIPAm systems to a variety of external factors, it is important to consider alternative explanations. Although NIPAm is sensitive to changes in temperature[55], pH[56], and solvent ionic strength[56,57], our observed increase in size is not accounted for by these factors. However, we considered that pH may partially or indirectly contribute to the observed swelling. Kratz et al.[56] demonstrated a size increase of NIPAm NPs containing low loadings (1.25 mol % and 12.5 mol %) of acrylic acid (AAc) at low pH above their LCST. Because the oxamate derivative incorporated into the polymer also has a carboxylic moiety, comparisons may be drawn between the 1.25 mol % loaded AAc NIPAm polymer and our system (OxNP). Kratz attributed this observation to an expected collapse (desolvation) above LCST, but the collapsed NPs were prone to form somewhat uniform aggregates at low pH.[56] This behavior was attributed to weak interparticle interactions. They also observed that this was completely reversible.

The pH of OxNP solutions drops significantly upon addition of lactic acid. If the observed swelling of OxNP-LDH complexes in 10 mM lactic acid was solely pH dependent, one would have expected OxNPs to have exhibited the same response when exposed to lactic acid at 37 ^{o}C. This, however, was not observed. Furthermore, at lactic acid concentrations similar to those found in healthy tissues in the body (1 mM), there is no response of OxNP-LDH complexes. Once lactic acid concentrations exceed the normal range, only NP-protein

complexes (OxNP-LDH) responded. We conclude therefore that the increase in size is due to a reduction in cross-linking brought about by competitive displacement of the polymer bound oxamate moiety by lactic acid.

Our main hypothesis is that lactic acid competitively displaces the polymer bound oxamate moiety, decreasing the cross-linking of the OxNP. However, due to the complexity of this system, it is not unreasonable to think that other factors might also contribute. For example, under 10 mM lactate conditions there could be "open" active binding sites on the homomeric tetramer LDH.[48] The generation of pyruvic acid within the OxNP could potentially contribute to swelling of particles since the K_d of pyruvate is similar to that of oxamate, this could displace more oxamate moieties and further increase swelling. Although this potential exists, this is not likely the most significant reason for swelling. Experiments involving OxNP and OxNP-LDH complexes with pyruvic acid led to irreversible aggregation of particles, unlike what was observed with lactic acid. This suggests there is something specific about lactic acid that does not lead to aggregation of particles, but instead leads to swelling.

Scanning Electron Microscopy Imaging of NPs

Scanning electron microscopy (SEM) was performed on OxNPs and lactic acid exposed OxNP-LDH complexes (Figure 6) to observe the size change of OxNP-LDH complexes in the

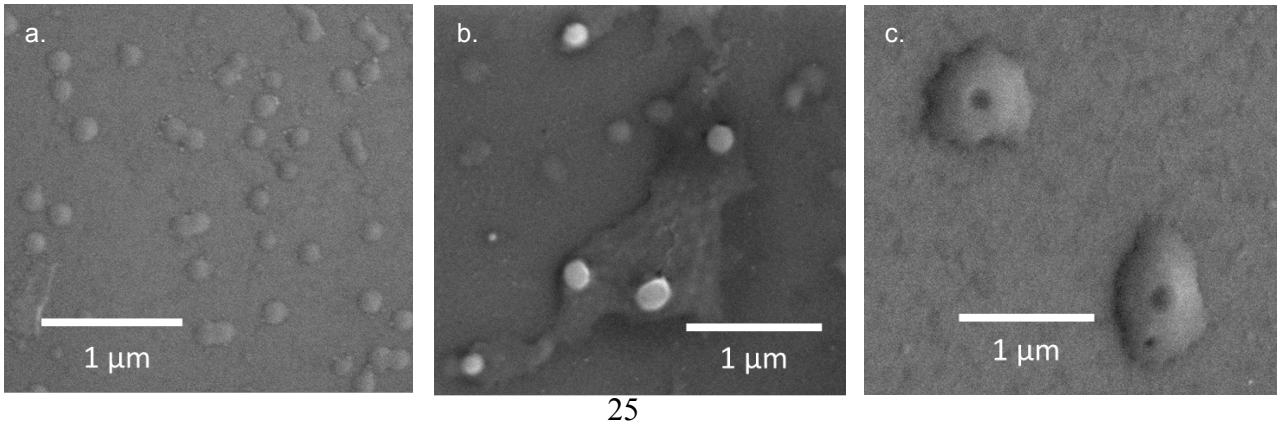

Figure 6: SEM images of OxNPs. Left: OxNPs alone (**a**). Middle: OxNPs with LDH (**b**). Right: OxNPs with LDH and lactic acid (**c**).

presence of 10 mM lactic acid. Samples were prepared by drop-casting a solution of OxNP in water onto glass slides then heated at 150 ^{o}C until dry. To establish a point of reference, SEM images were taken of OxNPs (Figure 6a). The size of OxNPs in Figure 6a and 6b (~ 160 nm) are roughly the same as those measured by DLS at 37 ^{o}C (183±1 nm). These images are consistent with the experimental results obtained by DLS for lactic acid responsiveness.

Cryo-Transmission Electron Microscope Images

To further characterize OxNP-LDH complexes, we employed cryo-transmission electron microscopy (cryoTEM) which enables the native state of the OxNPs to be imaged at high resolution (Figure 7).[58] Due to the 100-fold difference in density between OxNPs (0.01 g/mL) and LDH (1.3 g/mL), the contrast will be dominated by the LDH particles. At high defocus values (~10-20 microns), the OxNP-LDH complexes are easily identifiable and appear as homogeneous spheres with a 200 nm diameter (Figures 7a, highlighted with the dashed blue circles). This is consistent with the DLS measurements. At lower defocus values (~0.5 – 1 micron) the OxNP-LDH complexes display extremely low contrast (Figure 7b, highlighted by the dashed blue circles), but the resolution is sufficient to identify individual LDH particles (Figure 7c). Due to the superposition of the LDH particles it is only possible to measure their individual diameter (~ 8 nm) close to the edge of the structures[59], however, this is consistent with their previously measured R_H values (~ 4.3 nm)[60].

If LDH bound selectively to the surface, there would be a distinct and visible ring around the OxNPs; consequently, it was inferred that LDH distributed through the 3D volume of the OxNPs. This is consistent with our observation that OxNPs contract when exposed to LDH by 100 nm, and OxNP-LDH complexes swell when exposed to lactate. If LDH were confined to the surface of the OxNPs, cross-linking and subsequent swelling would be minimized.

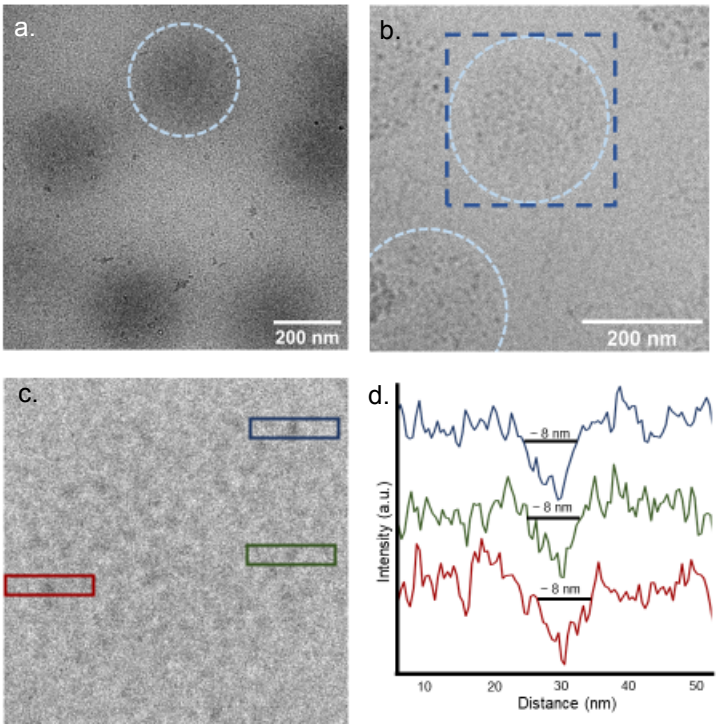

Figure 7: cryoTEM images of OxNPs and OxNP-LDH complexes. Top left: image of OxNPs cluster (a.) Top right: image of OxNPs with protein bound (b.) Bottom left: Magnification of blue box from (b.) showing discrete LDH particles (c.) Bottom right: plot profile of selected protein particles (d.)

Conclusions

In summary, a polymerizable oxamate LDH inhibitor **6** was synthesized and incorporated into lightly cross-linked NIPAm NPs, producing OxNPs. LDH was efficiently taken up into OxNPs in the solvent-swollen state through incubation and non-covalent binding to the polymer bound oxamate moieties in the polymer backbone. Protein loading was estimated to be 0.6 mg LDH/1 mg OxNP. CD was used to demonstrate that OxNPs do not lead to distortion or denaturation of LDH's secondary structure after being exposed to OxNPs below and above LCST as well as after one full heating cycle, which is important for cross-linking. OxNP-LDH complexes showed a large swelling response in the presence of high lactic acid concentrations (10 mM), but none at low lactic acid concentrations (1 mM). OxNP-LDH complexes exposed to lactic acid below LCST behave normally and remain the same size as without lactic acid. Above the LCST, lactic acid treated OxNP-LDH complexes swell almost double their size at room temperature. We have also used SEM to visualize OxNP-LDH complex's response to lactic acid. Through TEM, we have imaged OxNP-LDH complexes to further validate uptake. We conclude that we have developed a metabolite-responsive system. OxNP-LDH complexes swell in the presence of high lactic acid concentrations that mirror those found in tumors. The influence of temperature and lactic on particle swelling only influences OxNPs when they are complexed with LDH. This supports our hypothesis that LDH acts as a cross-linker within the polymer and is displaced in the presence of lactic acid. This system provides a platform for metabolite responsive NPs.

Acknowledgements

We gratefully acknowledge Laser Spectroscopy Laboratories at UC Irvine, and Q.N. Pham for his assistance with SEM.

Funding Sources

This work was funded by the University of California's Cancer Research Coordinating Committee (CTR-18-524776).

References

1. Xu, R.; Zhang, G.; Mai, J.; Deng, X.; Segura-Ibarra, V.; Wu, S.; Shen, J.; Liu, H.; Hu, Z.; Chen, L.; Huang, Y.; Koay, E.; Huang, Y.; Liu, J.; Ensor, J.E.; Blanco, E.; Liu, X.; Ferrari, M.; Shen, H. An injectable nanoparticle generator enhances delivery of cancer therapeutics. *Nat. Biotechnol.* **2016,** *34*, 414–418.
2. Kabanov, A. V., Bronich, T. K., Kabanov, V. A., Yu, K. & Eisenberg, A. Soluble stoichiometric complexes from poly(N□ethyl□4□vinylpyridinium) cations and poly(ethylene oxide)-block-polymethacrylate anions. *Macromolecules* **1996**, *29*, 6797–6802.
3. Harada, A. & Kataoka, K. Formation of polyion complex micelles in an aqueous milieu from a pair of oppositely-charged block copolymers with poly(ethylene glycol) segments. *Macromolecules* **1995**, *28*, 5294–5299.
4. Bae, Y., Fukushima, S., Harada, A. & Kataoka, K. Design of environment-sensitive Supramolecular assemblies for intracellular drug delivery: polymeric micelles that are responsive to intracellular pH change. *Angew. Chem. Int. Ed.* **2003**, *42*, 4640–4643.
5. Lee, Y.; Fukushima, S.; Bae, Y.; Hiki, S.; Ishii, T.; Kataoka, K. A protein nanocarrier from chargeconversion polymer in response to endosomal pH. *J. Am. Chem. Soc.* **2007**, *129*, 5362–5363.
6. Hartgerink, J. D., Beniash, E. & Stupp, S. I. Self-assembly and mineralization of peptide-amphiphile nanofibers. *Science* **2001**, *294*, 1684–1688.
7. Sun, W.; Jiang, T.; Lu, Y.; Reiff, M.; Mo, R.; Gu, Z. Cocoon-like self-degradable DNA nanoclew for anticancer drug delivery. *J. Am. Chem. Soc.* **2014**, *136*, 14722–14725.
8. Garbern, J. C., Minami, E., Stayton, P. S. & Murry, C. E. Delivery of basic fibroblast growth factor with a pH-responsive, injectable hydrogel to improve angiogenesis in infarcted myocardium. *Biomaterials* **2011**, 32, 2407–2416.
9. Pacardo, D. B., Ligler, F. S. & Gu, Z. Programmable nanomedicine: synergistic and sequential drug delivery systems. *Nanoscale* **2015**, *7*, 3381–3391.
10. Ling, D.; Park, W.; Park, S.J.; Lu, Y.; Kim, K.S.; Macket, M.J.; Kim, B.H.; Yim, H.; Jeon, Y.S.; Na, K.; Hyeon, T. Multifunctional tumor pH-Sensitive self-assembled nanoparticles for

bimodal imaging and treatment of resistant heterogeneous tumors. *J. Am. Chem. Soc.* **2014**, *136,* 5647–5655.
11. Chung, M.-F., Chia, W.-T., Wan, W.-L., Lin, Y.-J. & Sung, H.-W. Controlled release of an anti-inflammatory drug using an ultrasensitive ROS-responsive gas-generating carrier for localized inflammation inhibition. *J. Am. Chem. Soc.* **2015**, *137*, 12462–12465.
12. Callmann, C. E.; Barback, C.V.; Thompson, M.P.; Hall, D.J.; Mattrey, R.F.; Gianneschi, N.C. Therapeutic enzyme-responsive nanoparticles for targeted delivery and accumulation in tumors. *Adv. Mater.* **2015**, *27*, 4611–4615.
13. Zhang, S.; Ermann, J.; Succi, M.D.; Zhou, A.; Hamilton, M.J.; Cao, B.; Korzenik, J.R.; Glickman, J.N.; Vemula, P.K.; Glimcher, L.H.; Traverso, G.; Langer, R.; Karp, J.M. An inflammation-targeting hydrogel for local drug delivery in inflammatory bowel disease. *Sci. Transl. Med.* **2015***, 7*, 300ra128.
14. Kim, H.-J., Zhang, K., Moore, L. & Ho, D. Diamond nanogel-embedded contact lenses mediate lysozyme-dependent therapeutic release. *ACS Nano* **2014**, *8*, 2998–3005.
15. Jiang, T., Mo, R., Bellotti, A., Zhou, J. & Gu, Z. Gel– liposome-mediated co-delivery of anticancer membrane-associated proteins and small-molecule drugs for enhanced therapeutic efficacy. *Adv. Funct. Mater.* **2014**, *24*, 2295–2304.
16. Hu, Q.; Sun, W.; Lu, Y.; Bomba, H.N.; Ye, Y.; Jiang, T.; Isaacson, A.J.; Gu, Z. Tumor microenvironment-mediated construction and deconstruction of extracellular drug-delivery depots. *Nano Lett.* **2016**, *16*, 1118–1126.
17. Mo, R., Jiang, T., DiSanto, R., Tai, W. & Gu, Z. ATP-triggered anticancer drug delivery. *Nat. Commun.* **2014**, *5*, 3364-3373.
18. Wilson, W. R. & Hay, M. P. Targeting hypoxia in cancer therapy. *Nat. Rev. Cancer* **2011**, *11*, 393–410.
19. Holme, M. N.; Fedotenko, I.A.; Abegg, D.; Althaus, J.; Babel, L.; Favarger, F.; Reiter, R.; Tanasescu, R.; Zaffalon, P.L.; Ziegler, A.; Muller, B.; Saxer, T.; Zumbuehl, A. Shear-stress sensitive lenticular vesicles for targeted drug delivery. *Nat. Nanotechnol.* **2012**, *7*, 536–543.
20. Korin, N.; Kanapathipillai, M.; Matthews, B.D.; Crescente, M.; Brill, A.; Mammoto, T.; Ghosh, K.; Jurek, S.; Bencherif, S.A.; Bhatta, D.; Coskun, A.U., Feldman, C.L.; Wagner, D.D.; Ingber, D.E. Shear-activated nanotherapeutics for drug targeting to obstructed blood vessels. *Science* **2012**, *337*, 738–742.
21. McDaniel, J. R., Callahan, D. J.; Chilkoti, A. Drug delivery to solid tumors by elastin-like polypeptides. *Adv. Drug Deliv. Rev.* **2010**, *62*, 1456–1467.
22. Bae, Y. H., Okano, T., Hsu, R. & Kim, S. W. Thermo-sensitive polymers as on–off switches for drug release. *Makromol. Chem. Rapid Commun.* **1987**, *8*, 481–485.
23. Youn, Y.S.; Bae, Y.H. Perspectives on the past, present and future of cancer nanomedicine. *Advanced Drug Delivery Reviews* **2018**, *130*, 3-11.
24. Dunca, R. Polymer therapeutics at a crossroads? Finding the path for improved translation in the twenty-first century. *Journal of Drug Targeting* **2017**, *25*, 759-780.
25. Wang, T.; Ng, D. Y. W.; Wu, Y.; Thomas, J.; Tam Tran, T.; Weil, T., Bis-sulfide bioconjugates for glutathione triggered tumor responsive drug release. *Chem. Commun.*, **2014**, *50*, 1116-1118.
26. Stayton, P.S.; Shimoboji, T.; Long, C.; Chilkoti, A.; Ghen, G.; Harris, J.M.; Hoffman, A.S., Control of protein-ligand recognition using a stimuli-responsive polymer. *Nature*, **1995**, *378*, 472-474.

27. Huang, X.; Li, M.; Green, D.C.; Williams, D.S.; Tail, A.J.; Mann, S.; Interfacial assembly of protein-polymer nano-conjugates into stimulus-responsive biomimetic protocells. *Nature Commun.*, **2013**, *4*, 2239-2247.
28. Ge, J.; Neofytou, E.; Lei, J.; Beygui R.E.; Zare, R.N., Protein-polymer hybrid nanoparticles for drug delivery. *Small*, **2012**, *8*, 3573-3578.
29. Zhang, L.; Lu, Z.; Li, X.; Deng, Y.; Zhang, F.; Ma, C.; He, N., Methoxy poly(ethylene glycol) conjugated denatured bovine serum albumin micelles for effective delivery of camptothecin. *Polym. Chem.,* **2012**, *3*, 1958-1961.
30. Wu, Y.; Ihme, S.; Feuring-Buske, M.; Kuan, S.L.; Eisele, K.; Lamala, M.; Wang, Y.; Buske, C.; Weil, T., A core-shell albumin copolymer nanotransporter for high capacity loading and two-step release o doxorubicin with enhanced anti-leukemia activity. *Adv. Healtchare Mater.*, **2013**, *2*, 884-894.
31. Flenniken, M.L.; Liepold, L.O.; Crowley, B.E.; Willits, D.A.; Young, M.J.; Douglas, T., Selective attachment and release of a chemotherapeutic agent from the interior of a protein cage architecture. *Chem. Commun.*, **2005**, 447-449.
32. Ren, D.; Kratz, F.; Wang, S.W. Protein nanocapsules containing doxorubicin as a pH-responsive delivery system. Small, 2011, 7, 1051-1060.
33. Lu, Y.; Aimetti, A.A.; Langer, R.; Gu, Z., Bioresponsive materials. *Nature Reviews Materials*, **2016**, *2*, 1-17.
34. Heiden, M.G.V.; Cantley L.C.; Thompson C.B., Understanding the Warburg effect: the metabolic requirements of cell proliferation. *Science*, **2009**, *324*, 1029-1033.
35. Romero-Garcia, S., Moreno-Altamirano M.M.B., Prado-Garcia H., Sanchez-Garcia F.J., Lactate contribution to the tumor microenvironment: mechanisms, effects on immune cells and therapeutic relevance. *Front. Immunol.*, **2016**, *7*, 1-11.
36. Ward, P.S.; Thompson, C.B., Metabolic reprogramming: a cancer hallmark even Warburg did not anticipate. *Cancer Cell*, **2012**, *21*, 297-308.
37. Brooks, G.A., Lactate production under fully aerobic conditions – the lactate shuttle during rest and exercise. *Faseb J*, **1986**, *45*, 2924-2929.
38. West, J.B., Lactate during exercise at extreme altitude. *Faseb J,* **1986**, *45*, 2953-2957.
39. Shumer, W., Cell metabolism and lactate. *Lactate in Acute Conditions International Symposium*, **1978**, 1-9.
40. Walenta, S.; Wetterling, M.; Lehrke, M.; Schwickert, G.; Sundfor, K.; Rofstad, E.K.; Mueller-Klieser, W., High lactate levels predict likelihood of metastases, tumor recurrence, and restricted patient survival in human cervical cancers. *Cancer Res.*, **2000**, *60*, 916-921.
41. Roland, C.L.; Arumugam T.; Deng, D.F.; Liu, S.H.; Philip, B.; Gomex, S.; Burns, W.R.; Ramachandran, V.; Wang, H.M.; Cruz-Monserrate, Z.; Logsdon, C.D., Cell surface lactate receptor Gpr81 is crucial for cancer cell survival. *Cancer Res*, **2014**, *74*, 5301-5310.
42. Walenta, S.; Salameh A., Lyng, H.; Evensen, J.F.; Mitze, M.; Rofstad, E.K.; Meuller-Klieser, W., Correlation of high lactate levels in head and neck tumors with incidence of metastasis. *Am J. Pathol.*, **1997,** *150*, 409-415.
43. Brizel, D.M.; Schroeder T.; Scher, R.L.; Walenta, S.; Clough, R.W.; Dewhirst, M.W.; Meuller-Klieser, W., Elevated tumor lactate concentrations predict for an increased risk of metastases in head-and-neck cancer. *Int. J. Radiat. Oncol.*, **2001**, *51*, 349-353.
44. Yamagata, M., Hasuda K.; Stamato, T.; Tannock, I.F., The contribution of lactic acid to acidification of tumours: studies of variant cells lacking lactate dehydrogenase. *Brit. J. Cancer*, **1998**, *77*, 1726-1731.

45. O'Brien, J.; Shea, K. Tuning the Protein Corona of Hydrogel Nanoparticles: The Synthesis of Abiotic Protein and Peptide Affinity Reagents. *Accounts of Chemical Research*, **2016**, *49*, 1200−1210.
46. Dardonville C.; Fernandez-Fernandez C.; Gibbons S.L.; Ryan G.J.; Jagerovic N.; Gabilondo A.M.; Meana J.J.; Callado L.F., Synthesis and pharmacological studies of new hybrid derivatives of fentanyl active at the μ-opioid receptor and I2–imidazoline binding sites *Bioorg. Med. Chem*. **2006**, *14*,570-6580.
47. Dalmau, M.; Lim, S.; Chen, H. C.; Ruiz, C.; Wang, S. W. Thermostability and molecular encapsulation within an engineered caged protein scaffold. Biotechnol. Bioeng., 2008, 101, 654–664.
48. Clarke, A.R.; Wilks, H.M.; Barstow, D.A.; Atkinson, T.; Chia, W.N.; Holbrook, J.J., An investigation of the contribution made by the carboxylate group of an active site histidine-aspartate couple to binding and catalysis in lactate dehydrogenase. *Biochemistry*, **1988**, *27*, 1617-1622.
49. O'Carra, P.; Barry, S., Affinity Chromatography of Lactate Dehydrogenase, *FEBS Letters*, **1972**, *21*, 281-285.
50. Roop-ngam, P.; Thongboonkerd, V.; Development of an oxalate affinity chromatographic column to isolate oxalate-binding proteins, *Anal. Methods*, **2010**, *2*, 1051-1055.
51. Otsu, T.; Inoue, M.; Yamada, B.; Mori, T., Structure and reactivity of vinyl monomers: Radical reactivities of N-substituted acrylamides and methacrylamides. *Journal of Polymer Science: Polymer Letters Edition,* **1975**, *13*, 505-510.
52. Senff, H.; Richtering, W.; Influence of cross-link density on rheological properties of temperature-sensitive microgel suspensions, *Colloid. Polym. Sci,* **2000**, *278,* 830-840.
53. Hoshyar, N.; Gray, S.; Han, H.; Bao, G., The effect of nanoparticle size on *in vivo* pharmacokinetics and cellular interaction, *Nanomedicine (Lond).,* **2016**, *11*, 673-692.
54. Beardsley, D.S.; Kauzman, W.J., Local densities orthogonal to β-sheet amide planes: Patterns of packing in globular proteins, *Proc. Nat. Acad. Sci. USA*, **1996**, *93*, 4448-4453
55. Huffman, A.S.; Afrassiabi, A.; Dong, L.C., Thermally reversible hydrogels: II. Delivery and selective removal of substances from aqueous solutions. *J. Control. Release*, **1986***, 4, 213-222*.
56. Kratz, K.; Hellweg, T.; Eimer, W., *Colloids and Surfaces A: Physicochemical and Engineering Aspects*, Influence of charge density on the swelling of colloidal poly(*N*-isopropylacrylamide-co-acrylic acid) microgels, **2000**, *170*, 137-149.
57. Du, H.; Wickramasinghe, R.; Qian, X., Effects of salt on the lower critical solution temperature of Poly (N-Isopropylacrylamide). *J. Phys. Chem. B*, **2010**, *114*, 16594-16604.
58. Patterson, J. P.; Xu, Y.; Moradi, M. A.; Sommerdijk, N.; Friedrich, H., CryoTEM as an Advanced Analytical Tool for Materials Chemists, *Acc. Chem. Res*. **2017**, *50* 1495-1501.
59. van de Put, M. W.; Patterson, J. P.; Bomans, P. H.; Wilson, N. R.; Friedrich, H.; van Benthem, R. A.; de With, G.; O'Reilly, R. K.; Sommerdijk, N. A., Graphene oxide single sheets as substrates for high resolution cryoTEM. *Soft Matter,* **2015**, *11*, 1265-70.
60. Andersson, M.M.; Hatti-Kaul, R.; Brown, W. Dynamic and Static Light Scattering and Fluorescence Studies of the Interactions between Lactate Dehydrogenase and Poly(ethyleneimine), *J. Phys. Chem. B*, **2000**, *104*, 3660-3667.